# Graphene Isotope Superlattices with Strongly Diminished Thermal Conductivity for Thermoelectric Applications

Whiteway, Eric; Lee, Martin; Hilke, Michael

**DOI**
10.1021/acsanm.0c01802

**Publication date**
2020

**Document Version**
Accepted author manuscript

**Published in**
ACS Applied Nano Materials

# Graphene Isotope Superlattices with Strongly Diminished Thermal Conductivity For Thermoelectric Applications

Eric Whiteway,[†] Martin Lee,[†,‡] and Michael Hilke[*,†]

†*Department of Physics, McGill University, Montréal, Canada H3A 2T8*
‡*Kavli Institute of Nanoscience, Delft University of Technology, Lorentzweg 1, 2628 CJ, Delft, The Netherlands*

E-mail: hilke@physics.mcgill.ca

## Abstract

Graphene has a high intrinsic thermal conductivity and a high electron mobility. The thermal conductivity of graphene can be significantly reduced when different carbon isotopes are mixed, which can enhance the performance of thermoelectric devices. Here we synthesize isotopic $^{12}C/^{13}C$ random mixes and isotope superlattices with periods ranging from 46 to 225 nm by chemical vapour deposition. Raman Opto-Thermal conductivity measurements of these superlattice structures show an approximately 50% reduction in thermal conductivity compared to pristine $^{12}C$ graphene. This average reduction is similar to the random isotope mix. The reduction of the thermal conductivity in the superlattice is well described by a model of pristine graphene and an additional quasi-one dimensional periodic interfacial thermal resistance of $(2.5 \pm 0.5) \times 10^{-11}$ m$^2$K/W for the $^{12}C/^{13}C$ boundary. This is consistent with a large anisotropic thermal conductivity in the superlattice, where the thermal conductivity depends on the orientation of the $^{12}C/^{13}C$ boundary.

Keywords: Graphene, thermal conductivity, isotope superlattice, nanostructures, Raman spectroscopy, thermoelectric devices.

## Introduction

The novel electronic properties of graphene have produced a great deal of interest in the material for a number of applications.[1–3] Experimental results have indicated high thermal conductivity (2000-5000 W/m-K) for graphene[4–7] which could make it an important material for heat management in electronic devices. In areas such as solid state refrigeration and thermoelectric power generation it's desirable to have materials with a combination of high electrical conductivity and reduced thermal conductivity.[8] Isotope doped graphene demonstrates reduced thermal conductivity[4] and increased optical phonon scattering[9] without modifying electronic properties. The high carrier mobility of graphene (up to 200,000 cm$^2$V$^{-1}$s$^{-1}$)[10,11] as well as the measured Seebeck coefficient reported for graphene (50-100 $\mu$V/K at room temperature)[12,13] and predicted ultrahigh Seebeck coefficient in graphene nanostructures,[14] when combined with reduced thermal conductivity imposed by isotope impurities for could lead to a unique high performance material for thermoelectric devices.[15]

Isotope impurities reduce thermal conductivity through the mass difference phonon scattering of individual atoms. In two dimensions, the phonon contribution to the thermal conductivity is given by $K = \frac{1}{2} C v \lambda$, where $C$

is the specific heat capacity, $v$ is the phonon group velocity and $\lambda$ the phonon mean free path (mfp).[16] Substitution of isotope atoms leads to an increase in the phonon point-defect scattering rate and a corresponding reduction in phonon mfp. In the case of $^{12}C/^{13}C$ graphene and when considering only isotope substitution and neglecting coherence effects, we can express the inverse mfp as $\lambda^{-1} = \rho^{12}\lambda_{12}^{-1} + \rho^{13}\lambda_{13}^{-1} + \Gamma$, where $\lambda_{12} \simeq \lambda_0$ and $\lambda_{13} \simeq \lambda_0$ of the respective pure isotope lattices are similar and $\Gamma \sim \rho^{12}(1-M^{12}/\overline{M})^2 + \rho^{13}(1-M^{12}/\overline{M})^2$ where $\rho$ is the isotope concentration, $M$ is the isotope mass and $\overline{M}$ is the average mass.[4] The same is true for their respective group velocities and specific heat. Hence, the dependence of the thermal conductivity on isotopes is dominated by the term $\Gamma$, which leads to a maximum scattering rate at approximately 50% concentration. Thermal conductivity can also be reduced by the introduction of point defects and vacancies, which lead to stronger scattering due to the increased mass difference term.[17]

The situation for synthesized ordered isotope superlattices (SLs) is different (Figure 1), since there are no random impurities. However, isotopic SLs are expected to have reduced thermal conductivities[18] and were shown by simulations to have a dependence on the superlattice period, with a minimum thermal conductivity corresponding to the crossover between coherent and incoherent phonon transport, estimated at 6.25 nm.[19]

At large periods, exceeding the phonon coherence length, the SL acts as a series of independent barriers, characterized by an interface density, $I_d = \frac{1}{L_s}$ orthogonal to the periodicity. The thermal resistance is then expected to be proportional to $\sim I_d R_I$, where $R_I$ is the interfacial thermal resistance (Kapitza resistance) at the $^{12}C/^{13}C$ boundary.[19,20]

This breaks down when the SL period is smaller than the phonon coherence length, In the coherent regime the SL can no longer be seen as independent scatterers, but rather as a hybridized supercell, which leads to an expected increase in thermal conductivity relative to the superlattice minimum.[18] This behaviour has been observed in experimental studies of

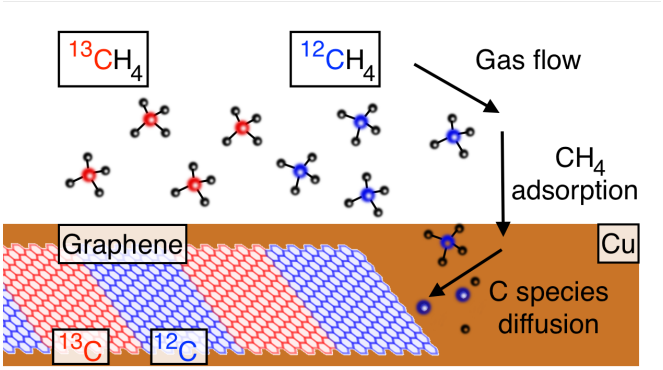


Figure 1: Isotope superlattice synthesis by alternating pulses of $^{12}CH_4$ and $^{13}CH_4$ gas flow during CVD growth. Growth proceeds by adsorption and catalytic decomposition of methane into carbon species which diffuse along the copper surface and attach to the graphene crystal edge.

three dimensional systems[21–25] and reported in MD[19,26–28] and NEGF[15] studies of graphene isotope superlattices and other 2D systems.[29,30] This is yet to be experimentally verified in 2D materials due to the difficulty in synthesizing periodic superlattices at relevant length scales.

Here we report the thermal conductivity measurements of graphene monocrystals synthesized by chemical vapor deposition with an artificial isotope SL with periods $L_s$ ranging from 46 to 225 nm. Because of the much smaller phonon coherence length than $L_s$, we expect the SL to be in the incoherent phonon transport regime,[19] which is dominated by the added interfacial thermal resistance at each half period. We therefore expect the thermal conductivity to monotonically decrease with increased interface density, $I_d$. Our theoretical model and simulations of heat transport agree well with the experimental outcome. We demonstrate that at the smallest SL period, the thermal conductivity is reduced by ~50%. This is an important step towards further optimizing the thermal properties of graphene without sacrificing the electronic properties.

## Results and Discussion

The sample studied contains 6 distinct regions each corresponding to a unique isotope dosing sequence. After transfer to an Au covered holey SiN substrate the sample was characterized by Raman mapping and the average SL periods $L_s$ were determined to be 46, 75, 117, and 225 nm for the 4 SL regions. The Raman spectra of different regions of the sample reflect their isotope distribution (see Figure 2). For the pure $^{12}$C region we observe a single narrow Lorentzian G or 2D-peak, whereas for the 50% we observe significant broadening consistent with an increase in phonon scattering[9] (see Figures 2 and 3). In the superlattice regions we observe a double peak structure which is roughly the sum of the bulk $^{12}$C and $^{13}$C Raman spectra. This indicates the formation of a heterogeneous isotope distribution with a periodic variation in the phonon local density of states. This also shows that the optical phonon coherence length is smaller than the superlattice period, otherwise hybridization of the phonon bands would occur, which would narrow the separation between the heterogeneous Raman peaks.

Thermal conductivity of the sample in Figure 4 was measured using the Raman opto-thermal technique as previously described.[4–6,32,33] Heating the sample results in a laser power dependent Raman shift as shown in Figure 3.

In the case of pure $^{12}$C graphene we obtain a value of $K = 3200 \pm 1200$ W/m-K. We observe a reduction in the thermal conductivity for both the homogeneous isotope mixtures of 1800±600 W/m-K for 50% $^{12}$C and the periodic superlattices with $L_s$ from 46-225 nm where we find $K$ between 1700 and 2100 W/m-K. These values correspond to the lowest temperature measurement and cover a range from approximately 316-335 K, where it largely follows an inverse temperature dependence (Figure S1). The measured thermal conductivity temperature dependence is shown in Figure 4a. These values are consistent with previous reports for both 100% and 50% $^{12}$C which were reported as 4120 and 1977 W/m-K respectively[4] at similar temperatures. In comparison, introduction of defects by electron beam irradiation has been shown

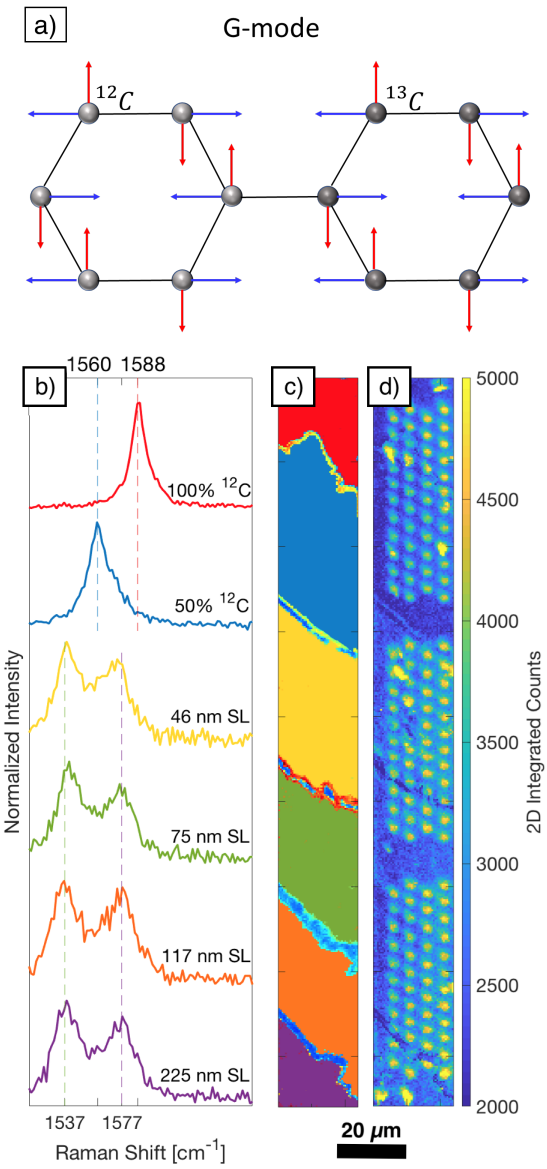


Figure 2: a) G-mode vibrations at the Γ point with $^{12}$C and $^{13}$C isotopes. The red and blue arrows correspond to the two polarizations. b) Raman G peak for 6 distinct regions of Isotope superlattice sample. Vertical dashed lines show the G peak position for each distribution at 1537/1577 cm$^{-1}$ for the SL regions (bottom), 1560 cm$^{-1}$ for the 50% $^{12}$C and 1588 cm$^{-1}$ for 100% $^{12}$C (top). c) Corresponding regions in Raman map (false colour) d) Integrated 2D peak counts Raman maps of graphene on holey membrane. Suspended graphene shows an increase in 2D peak intensity consistent with previous results showing increase 2D peak intensity for suspended vs supported graphene.[31]

to reduce thermal conductivity of suspended graphene to ∼400 W/m-K..[17] The thermal conductivity values as a function of heating power are tabulated in Table 1.

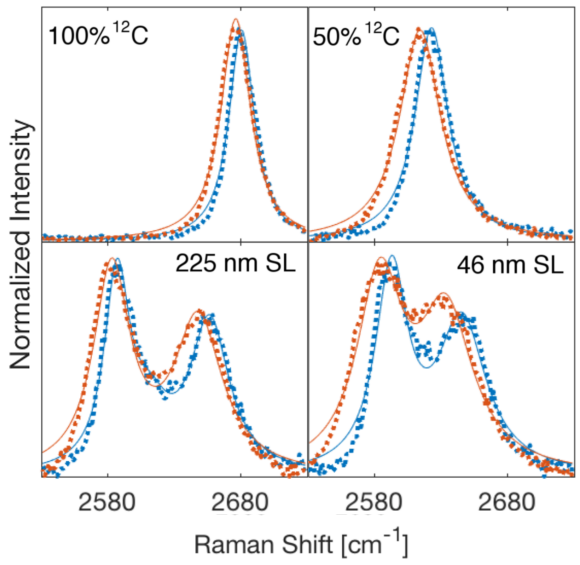


Figure 3: 2D peak Raman spectra for high (red) and low (blue) power laser excitations. The dots are the experimental spectra, while the lines correspond to Lorentzian fits. We give the approximate 2D peak positions for (low→high) power. The top left is for pure $^{12}$C (2680 → 2676 cm$^{-1}$), top right for the homogeneous $^{12}$C-$^{13}$C mix (2622 → 2614 cm$^{-1}$), bottom left for the 225 nm period (2656/2588 → 2650/2582 cm$^{-1}$), and bottom right the 46 nm period (2637/2597 → 2628/2588 cm$^{-1}$). The magnitude of the shift in peak position (red vs blue) is proportional to the graphene membrane temperature. We note that for small superlattice periods the lineshape and apparent positions of the 2D peak are modified by the presence of an emergent intermediate Raman peak[34] but that this does not affect the temperature measurement, which depends only on the relative shift of the entire peak structure.

We note that a large part the quoted uncertainty on the thermal conductivity is due to the experimental uncertainty inherent to the Raman opto-thermal technique which is sensitive to the laser power output, graphene optical absorption, laser spot size and sample geometry and is dependent on the assumptions made in extracting the thermal conductivity from the measured spectrum. As a result experimental values of thermal conductivity of suspended graphene measured by opto-thermal techniques cover a range from approx. 600 - 5000 W/m-K,[8,33] which reflects both sample quality variance and measurement technique differences in various experimental setups. Li et al. developed a technique to extract thermal conductivity independent of absorbed power by modifying laser spot size and find a value of thermal conductivity approx 1500 W/m-K[33] for single layer graphene.

While the absolute uncertainty in thermal conductivity is quite large, the relative uncertainty between different structures is minimal. This is because we measure a single graphene crystal[35,36] and measure multiple spots in each region with the same circular hole geometry (∼ 10 spots per region). The uncertainty in the relative values of $K$, determined from the std. error, then, are considerably smaller and the effect of systematic errors involved with Raman opto-thermal measurements are minimized. In Figure 4b the error bars show the standard error and reflect the relative errors between data points.

In the case of the superlattice samples the assumption of isotropic heat conduction is no longer valid and we should not expect a uniform value of $K$. In fact the thermal resistance may vary significantly when measured in perpendicular and parallel directions relative to the mass periodicity. To first order we expect the effective thermal resistance for a distance $R$ in direction $\theta$ to be given by $R_{eff}(\theta) = R_g + \cos(\theta)\frac{2R}{L_s}R_{int}$, where $R_g = RK_g^{-1}$ is the thermal resistance of pristine graphene, $K_g$ the thermal conductivity of pristine graphene, and $R_{int}$ the interfacial resistance (the average between the $^{12}$C-$^{13}$C and $^{13}$C-$^{12}$C interface). Here $\theta = 0$ is the direction perpendicular to the $^{12}$C-$^{13}$C interface. This expression assumes that the total scattering rate is simply the sum of the pristine graphene rate and the interfacial rate, which depends on the orientation of the interface. To obtain an estimate for our circular geometry, we have to average over the same geometry. This can be done by integrating the ther-

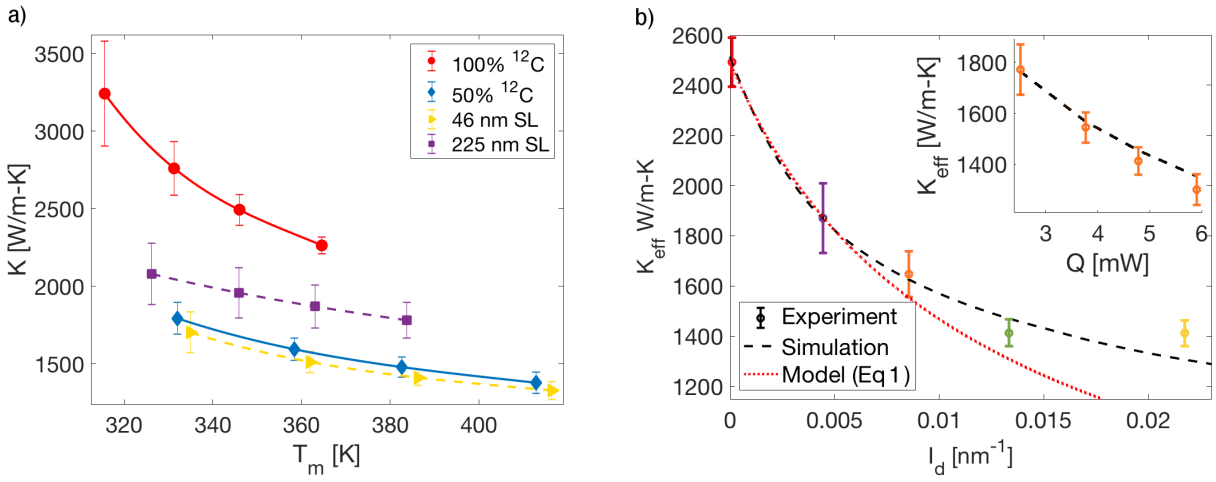


Figure 4: a) Temperature dependence of the thermal conductivity of suspended graphene sheet with various $^{12}$C/$^{13}$C isotope concentrations and distributions. (75 and 117 nm superlattices are omitted for clarity) b) Effective thermal conductivity as a function of interface density. Data points represent a single fixed heating power (4.78 mW). The dashed line shows the value of $K_{eff}$ determined from simulation setting $K_g = 2492$ W/m-K, and $R_{int} = 2.4 \times 10^{-11}$ m$^2$K/W. The dotted line corresponds to equation (1) with the same parameters. The inset shows the dependence on heating power $Q$ for $L_s = 117$ nm compared to the simulation (assuming a temperature independent $R_{int}$.

mal conductivity over all directions ($\theta$). This implies integrating the inverse of the effective resistance over $\theta$, which leads to the arctan expression in (1).

$$K_{eff} \simeq \frac{2L_s}{\pi R_{int}} \frac{\arctan\sqrt{\frac{a-1}{a+1}}}{\sqrt{a^2-1}} \qquad (1)$$

where $R$ is also the radius of the suspended graphene and $a = L_s/(2R_{int}K_g)$. We expect this to be a good approximation for large periodicities ($L_s \gg r_0$), where $r_0$ is the laser spot size.

To obtain a more detailed picture taking into account the finite laser spot size and the non-uniform heat flow, we use the relaxation method to solve the inhomogeneous heat equation:

$$-\nabla \cdot (K(x,y)\nabla T) = \dot{q}, \qquad (2)$$

where $\dot{q}$ is the volumetric heat source.

In Figure 5 we show the temperature map across a homogeneous graphene membrane and a membrane with periodic interfaces with $L_s$ of 225 nm from simulation. We observe in the superlattice sample an increase in temperature of the film relative to the isotopically pure case, particularly at the center where $\dot{q}$ is highest. The temperature rise in the simulation is consistent with the observed experimental results. The circular symmetry of the heat conduction is also disrupted, and discrete temperature drops are evidenced at the isotope boundaries.

When comparing the extracted thermal conductivity from the opto-thermal measurements and the simulation we find a good agreement as shown in Figure 4b. The initial slope agrees well with the estimate in equation (1) for large periods (225 nm). For smaller periods there is a systematic deviation between the simulation and (1), which is due to the finite size of the heating area (laser spot size), where the simulation is closer to the experimental dependence. However, for the smallest period (46 nm) the experimental conductivity is larger than the value obtained by the simulation. This could be due to the coherence effects mentioned earlier, but is more likely due to the increased mixing of $^{12}$C in the $^{13}$C phase and vice versa. In fact, molecular dynamics studies of the thermal conductivity of a graphene isotope SL suggest that thermal conductivity can be further reduced by substituting additional isotope atoms on top of the periodic structure.[28] However in

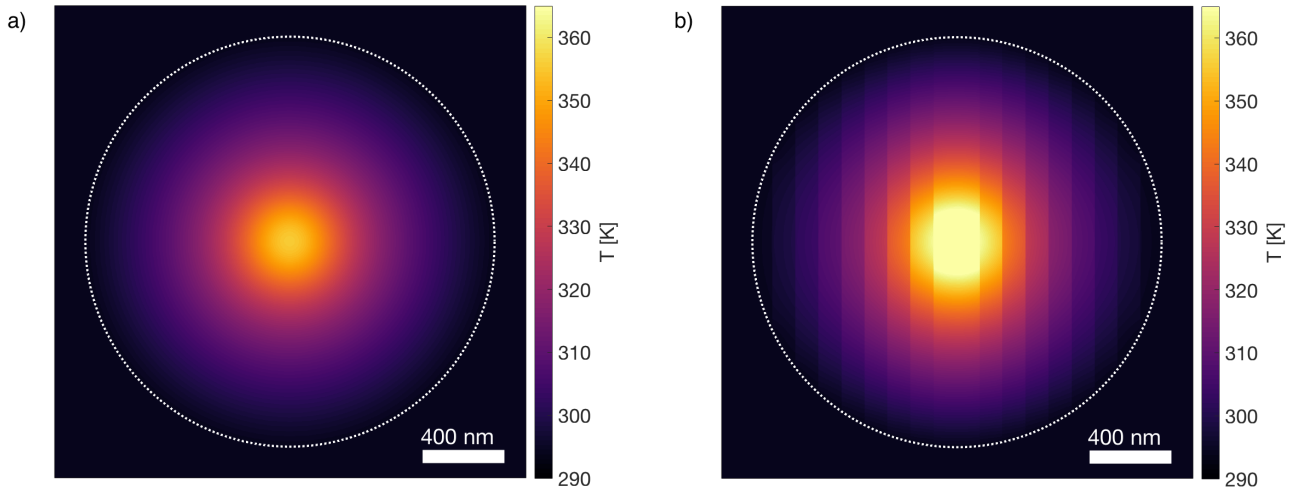


Figure 5: Suspended graphene membrane temperature from simulation for $^{12}$C graphene and 225 nm periodic superlattice with $Q = 4.78$ mW heat source. Dashed line represents the boundary between the suspended and supported graphene. We find $T_m = 345$ K and $T_m = 363$ K for the $^{12}$C and 225 nm SL respectively. $K_g$ is taken to be the experimentally value 2492 W/m-K and $R_{int}$ is determined to be $2.4 \times 10^{-11}$ m$^2$K/W

a SL there is a trade-off between decreasing bulk conductivity by isotope impurities and increasing interface thermal conductance by reducing the mass difference between alternating isotope layers. Therefore at small periods isotope doping could lead to the observed increase in thermal conductivity. The total thermal resistance increase, is therefore a combination of residual isotope doping and interfacial thermal resistance.

Figure 4b shows the effective thermal conductivity $K_{eff}$ given by equation 3, where the heat source $Q$ and measured temperature $T_m$ are both given by a Gaussian beam profile with diameter $D = 340$ nm. These are compared to the experimentally measured values of $K_{eff}$ for the equivalent fixed laser power. The thermal conductivity of the film is taken as the experimental value $K_g = 2492$ W/m-K and the best fit is obtained for an interfacial thermal resistance of $R_{int} = (2.4 \pm 0.7) \times 10^{-11}$ m$^2$K/W. The value of $R_{int}$ varies depending on laser power, as shown in table 1, from 2.0-3.2 $\times 10^{-11}$ m$^2$K/W. We also note that as a consequence of the CVD growth process the synthesized isotope interfaces are not atomically sharp and as such the value of the thermal interface resistance may vary depending on the exact structure of the isotope boundary. For the full range of experimental data, independent of laser power, the best fit is calculated as $R_{int} = (2.5 \pm 0.5) \times 10^{-11}$ m$^2$K/W, which is comparable to the values found by non-equilibrium molecular dynamics studies, which find a thermal resistance of a graphene $^{12}$C/$^{13}$C interface as $1.05 \times 10^{-11}$ m$^2$K/W[19] and $3.88 \times 10^{-11}$ m$^2$K/W.[20]

# Conclusions

The thermal conductivity of various isotope distributions in graphene show a reduction in thermal conductivity for both homogeneous isotope mixtures and superlattices. For pure $^{12}$C graphene we measure thermal conductivity as high as 3200 W/m-K. In the case of periodic superlattices, the thermal conductivity decreases with increased interface density. The isotope interfacial thermal resistance is found to be $(2.5 \pm 0.5) \times 10^{-11}$ m$^2$K/W. In a polar geometry this leads to an almost factor 2 reduction in the thermal conductivity, while across the interfaces this reduction is even larger. This would strongly reduce the thermal conductivity of a nanoribbon in the direction transverse to the superlattice. In comparison to random isotope

Table 1: Measured temperature and corresponding thermal conductivity for different isotope distributions

| | **100% $^{12}$C** | | **50% $^{12}$C** | | **46 nm SL** | | **75 nm SL** | | **117 nm SL** | | **225 nm SL** | | $\mathbf{R_{int}}$ |
|---|---|---|---|---|---|---|---|---|---|---|---|---|---|
| Q [mW] | $T_m$[K] | K [W/m-K] | $T_m$[K] | K [W/m-K] | $T_m$[K] | K [W/m-K] | $T_m$[K] | K [W/m-K] | $T_m$[K] | K [W/m-K] | $T_m$[K] | K [W/m-K] | [m$^2$K/W] |
| 2.50 | *316* | 3242 | *332* | 1793 | *335* | 1703 | *333* | 1770 | *332* | 1797 | *326* | 2080 | $3.2\times10^{-11}$ |
| 3.77 | *331* | 2760 | *358* | 1595 | *362* | 1513 | *360* | 1544 | *356* | 1692 | *346* | 1958 | $2.7\times10^{-11}$ |
| 4.78 | *346* | 2492 | *383* | 1480 | *386* | 1412 | *386* | 1414 | *374* | 1647 | *363* | 1870 | $2.4\times10^{-11}$ |
| 5.90 | *365* | 2265 | *413* | 1379 | *416* | 1329 | *418* | 1301 | *395* | 1625 | *384* | 1782 | $2.0\times10^{-11}$ |

doping, where the minimum thermal conductivity is limited and isotropic, isotope superlattices may be able to achieve further reductions by reducing the superlattice period, modifying the level of residual isotope doping or introducing quasi-periodic structures. We also expect a similar reduction for large polycrystalline CVD grown graphene superlattices, where interface orientation is randomized. The observed reduction in thermal conductivity can lead to interesting applications for thermoelectric devices that need high electrical conductivities with low thermal conductivities.

# Methods

## Synthesis

Superlattice synthesis was accomplished by chemical vapour deposition, alternatively pulsing $^{12}$C and $^{13}$C methane gases on ∼1 second timescales. Graphene CVD substrate was a commercially available 25 $\mu$m thick copper foil and gas stock consisted of $^{12}$C methane (99.99% purity) or $^{13}$C-methane (99.9% purity) from Cambridge Isotopes Laboratories (CLM-3590-1). Detailed description of the CVD system and growth procedures have been previously reported[36] based on established techniques.[37] The resulting graphene single crystals were transferred using a typical PMMA wet transfer technique to either $Si/SiO_2$ wafers or holey SiN substrates for analysis by Raman spectroscopy.

Results are based on a single sample divided into 6 distinct regions corresponding to, pure $^{12}$C, 50% $^{12}$C-$^{13}$C mix, and 4 SLs of varying periodicity. The regions are separated by small regions of pure $^{12}$C or $^{13}$C graphene. Figure 6 shows a typical gas flow sequence along with the associated isotope distribution as a function of

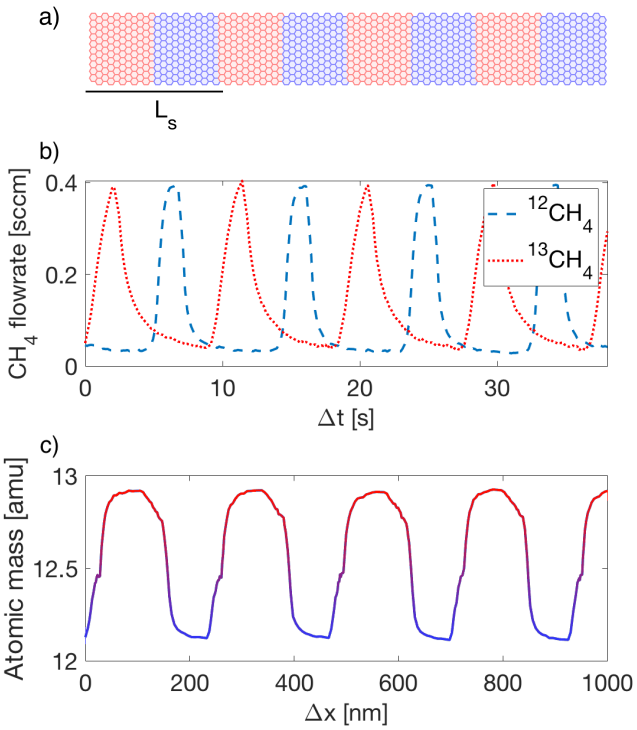


Figure 6: Top: illustration of a graphene isotope superlattice with period $L_s$ of 5nm, where the blue regions correspond to $^{12}$C and the red regions to $^{13}$C. Growth log showing flowrates $\dot{V}$ of $^{12}$C and $^{13}$C methane along with the corresponding atomic mass vs. distance where distance is calculated as $\dot{V}\Delta t$ and scaled to correspond to the measured growth rate and atomic mass is measured as a function of isotopic methane concentration.

radial distance for the SL region.

We note that as a result of the non-zero rise and fall times of the isotopic gas flow we do not achieve atomically sharp interfaces nor isotopically pure bands in the superlattice regions. From the measured isotopic gas flow we estimate the maximum concentration of 89-92% isotope concentration for the $^{12}$C and $^{13}$C bands respectively.

## Opto-Thermal Conductivity measurement

Graphene superlattices were suspended on gold covered holey SiN membranes and a Raman opto-thermal technique was employed to determine thermal conductivity. A Renishaw Invia Raman system and a 514 nm laser excitation source was used for spectroscopy and as a heating element for the suspended graphene sheet. The temperature dependence of the Raman 2D peak shift is used to measure the local temperature rise in the suspended film and the dependence of this temperature rise on absorbed laser power is used to extract the thermal conductivity. The details of the thermal conductivity measurement were based off the approach of Cai et al[32] and Chen et. al[4] who used a similar arrangement of Au covered holey SiN membranes to measure the thermal conductivity of various isotopic mixes. The 2D peak temperature dependence is taken as $-7.23 \times 10^{-2}\, cm^{-1}/K$ for $^{12}$C graphene and $-6.98 \times 10^{-2}\, cm^{-1}/K$ for the 50% mix and superlattice samples.[4] We similarly use a value for laser absorption of 3.4% and a laser spot size of 340 nm. The thermal conductivity is then obtained as:

$$K = \alpha \frac{ln\left(\frac{R}{r_0}\right)}{2\pi t R_g} \tag{3}$$

Where $R = 1\,\mu$m is the radius of the hole, $r_0 = 170$ nm is the radius of the laser spot, $t = 3.4$ Å is the thickness of the graphene film and $R_g$ is the measured thermal resistance. $\alpha = 0.96$ is a constant that is a function of $R$ and $r_0$.[32]

$$R_g = \frac{T_m - T_a}{Q_{abs}} \tag{4}$$

Where $T_m$ is the measured temperature of the film and $T_a$ is the ambient temperature. We neglect heat loss to the environment and thermal contact resistance between the graphene and the gold substrate. In Figure S2 we show a scanning electron microscopy image of the holey SiN membrane covered by a graphene flake.

## Heat flow simulation

The temperature is evaluated numerically using the relaxation method on a rectangular grid with spacing $h = 1$ nm. Setting the initial temperature of the system at $T = 293$ K and holding the boundary temperature fixed, the interior grid points are determined iteratively by:

$$T_i^* = \sum_{\langle ij \rangle} \frac{K_j T_j}{\overline{K}_i} + h^2 \frac{\dot{q}_i}{K_i} \tag{5}$$

Where we have $\overline{K}_i = \sum_{\langle ij \rangle} K_j$ is the average thermal conductivity of the four nearest neighbours to i.

The periodicity dependence was modeled by considering a fixed graphene membrane thermal conductivity, $K_g$ with periodic interfaces represented by 1 nm strips with thermal resistivity $K_{int} = h/R_{int}$. We consider a circular suspended graphene membrane with radius $R = 1\,\mu$m and thermal conductivity $K_g$ attached to a rectangular heatsink with thermal conductivity $K_{hs} \gg K_g$ for $R > 1\mu$m.

## Supporting Information

Additional figures showing the thermal conductivity of SLs as a function of inverse temperature and scanning electron microscopy images of a graphene coated device.

# Acknowledgments:

We thank Jesse Maassen for helpful discussionss. This work was supported by NSERC, FRQNT, RQMP, CPM and INTRIQ.

# References


1. Novoselov, K. S.; Geim, A. K.; Morozov, S. V.; Jiang, D.; Katsnelson, M. I.; Grigorieva, I. V.; Dubonos, S. V.; Firsov, A. A. Two-dimensional gas of massless Dirac fermions in graphene. Nature **2005**, 438, 197–200.

2. Geim, A. K. Graphene: Status and Prospects. Science **2009**, 324, 1530–1534.

3. Cooper, D. R.; D'Anjou, B.; Ghattamaneni, N.; Harack, B.; Hilke, M.; Horth, A.; Majlis, N.; Massicotte, M.; Vandsburger, L.; Whiteway, E.; Yu, V. Experimental Review of Graphene. ISRN Condensed Matter Physics **2012**, 2012, 501686.

4. Chen, S.; Wu, Q.; Mishra, C.; Kang, J.; Zhang, H.; Cho, K.; Cai, W.; Balandin, A. A.; Ruoff, R. S. Thermal conductivity of isotopically modified graphene. Nature Materials **2012**, 11, 203–207.

5. Balandin, A. A.; Ghosh, S.; Bao, W.; Calizo, I.; Teweldebrhan, D.; Miao, F.; Lau, C. N. Superior Thermal Conductivity of Single-Layer Graphene. Nano Letters **2008**, 8, 902–907.

6. Ghosh, S.; Calizo, I.; Teweldebrhan, D.; Pokatilov, E. P.; Nika, D. L.; Balandin, A. A.; Bao, W.; Miao, F.; Lau, C. N. Extremely high thermal conductivity of graphene: Prospects for thermal management applications in nanoelectronic circuits. Applied Physics Letters **2008**, 92, 151911.

7. Balandin, A. A. Phononics of Graphene and Related Materials. ACS Nano **2020**, 14, 5170–5178, PMID: 32338870.

8. Nika, D. L.; Balandin, A. A. Phonons and thermal transport in graphene and graphene-based materials. Reports on Progress in Physics **2017**, 80, 036502.

9. Rodriguez-Nieva, J. F.; Saito, R.; Costa, S. D.; Dresselhaus, M. S. Effect of $^{13}$C isotope doping on the optical phonon modes in graphene: Localization and Raman spectroscopy. Physical Review B **2012**, 85, 245406.

10. Novoselov, K. S.; Geim, A. K.; Morozov, S. V.; Jiang, D.; Zhang, Y.; Dubonos, S. V.; Grigorieva, I. V.; Firsov, A. A. Electric Field Effect in Atomically Thin Carbon Films. Science **2004**, 306, 666–669.

11. Bolotin, K. I.; Sikes, K. J.; Jiang, Z.; Klima, M.; Fudenberg, G.; Hone, J.; Kim, P.; Stormer, H. L. Ultrahigh electron mobility in suspended graphene. Solid State Communications **2008**, 146, 351–355.

12. Zuev, Y. M.; Chang, W.; Kim, P. Thermoelectric and Magnetothermoelectric Transport Measurements of Graphene. Phys. Rev. Lett. **2009**, 102, 096807.

13. Seol, J. H.; Jo, I.; Moore, A. L.; Lindsay, L.; Aitken, Z. H.; Pettes, M. T.; Li, X.; Yao, Z.; Huang, R.; Broido, D.; Mingo, N.; Ruoff, R. S.; Shi, L. Two-Dimensional Phonon Transport in Supported Graphene. Science **2010**, 328, 213–216.

14. Dragoman, D.; Dragoman, M. Giant thermoelectric effect in graphene. Applied Physics Letters **2007**, 91, 203116.

15. Ouyang, T.; Chen, Y. P.; Yang, K. K.; Zhong, J. X. Thermal transport of isotopic-superlattice graphene nanoribbons with zigzag edge. Europhysics Letters **2009**, 88, 28002.

16. Nika, D. L.; Balandin, A. A. Two-dimensional phonon transport in graphene. Journal of Physics: Condensed Matter **2012**, 24, 233203.

17. Malekpour, H.; Ramnani, P.; Srinivasan, S.; Balasubramanian, G.; Nika, D. L.; Mulchandani, A.; Lake, R. K.; Balandin, A. A. Thermal conductivity of graphene with defects induced by electron

beam irradiation. Nanoscale **2016**, 8, 14608–14616.

18. Simkin, M. V.; Mahan, G. D. Minimum Thermal Conductivity of Superlattices. Physical Review Letters **2000**, 84, 927–930.

19. Mu, X.; Zhang, T.; Go, D. B.; Luo, T. Coherent and incoherent phonon thermal transport in isotopically modified graphene superlattices. Carbon **2015**, 83, 208–216.

20. Pei, Q.-X.; Zhang, Y.-W.; Sha, Z.-D.; Shenoy, V. B. Carbon isotope doping induced interfacial thermal resistance and thermal rectification in graphene. Applied Physics Letters **2012**, 100, 101901.

21. Lee, S. M.; Cahill, D. G.; Venkatasubramanian, R. Thermal conductivity of Si–Ge superlattices. Applied Physics Letters **1997**, 70, 2957–2959.

22. Venkatasubramanian, R. Lattice thermal conductivity reduction and phonon localizationlike behavior in superlattice structures. Physical Review B **2000**, 61, 3091–3097.

23. Borca-Tasciuc, T.; Liu, W.; Liu, J.; Zeng, T.; Song, D. W.; Moore, C. D.; Chen, G.; Wang, K. L.; Goorsky, M. S.; Radetic, T.; Gronsky, R.; Koga, T.; Dresselhaus, M. S. Thermal conductivity of symmetrically strained Si/Ge superlattices. Superlattices and Microstructures **2000**, 28, 199–206.

24. Watanabe, H.; Shikata, S. Superlattice structures from diamond. Diamond and Related Materials **2011**, 20, 980–982.

25. Ravichandran, J.; Yadav, A. K.; Cheaito, R.; Rossen, P. B.; Soukiassian, A.; Suresha, S. J.; Duda, J. C.; Foley, B. M.; Lee, C.-H.; Zhu, Y.; Lichtenberger, A. W.; Moore, J. E.; Muller, D. A.; Schlom, D. G.; Hopkins, P. E.; Majumdar, A.; Ramesh, R.; Zurbuchen, M. A. Crossover from incoherent to coherent phonon scattering in epitaxial oxide superlattices. Nature Materials **2013**, 13, 168–172.

26. Hu, J.; Schiffli, S.; Vallabhaneni, A.; Ruan, X.; Chen, Y. P. Tuning the thermal conductivity of graphene nanoribbons by edge passivation and isotope engineering: A molecular dynamics study. Applied Physics Letters **2010**, 97, 133107.

27. Davies, M.; Ganapathysubramanian, B.; Balasubramanian, G. Optimizing isotope substitution in graphene for thermal conductivity minimization by genetic algorithm driven molecular simulations. Applied Physics Letters **2017**, 110, 133107.

28. Gu, Y. Phonon thermal transport in semi-disordered isotopic-superlattice graphene nanoribbons. Numerical Heat Transfer, Part A: Applications **2018**, 73, 115–124.

29. Xie, Z.; Chen, X.; Yu, X.; Zhang, Y.; Wang, H.; Zhang, L. Reduction of phonon thermal conduction in isotopic graphene nanoribbon superlattices. Science China Physics, Mechanics & Astronomy **2017**, 60, 107821.

30. Felix, I. M.; Pereira, L. F. C. Thermal Conductivity of Graphene-hBN Superlattice Ribbons. Scientific Reports **2018**, 8, 2737.

31. Ni, Z. H.; Yu, T.; Luo, Z. Q.; Wang, Y. Y.; Liu, L.; Wong, C. P.; Miao, J.; Huang, W.; Shen, Z. X. Probing Charged Impurities in Suspended Graphene Using Raman Spectroscopy. ACS Nano **2009**, 3, 569–574.

32. Cai, W.; Moore, A. L.; Zhu, Y.; Li, X.; Chen, S.; Shi, L.; Ruoff, R. S. Thermal Transport in Suspended and Supported Monolayer Graphene Grown by Chemical Vapor Deposition. Nano Letters **2010**, 10, 1645–1651.

33. Li, Q.-Y.; Xia, K.; Zhang, J.; Zhang, Y.; Li, Q.; Takahashi, K.; Zhang, X. Measurement of specific heat and thermal conductivity of supported and suspended graphene

by a comprehensive Raman optothermal method. Nanoscale **2017**, 9, 10784–10793.

34. Whiteway, E.; Lee, M.; Hilke, M. Real Space Raman Spectroscopy of Graphene Isotope Superlattices. arXiv preprint arXiv:2007.12272 **2020**,

35. Massicotte, M.; Yu, V.; Whiteway, E.; Vatnik, D.; Hilke, M. Quantum Hall effect in fractal graphene: growth and properties of graphlocons. Nanotechnology **2013**, 24, 325601.

36. Whiteway, E.; Yang, W.; Yu, V.; Hilke, M. Time evolution of the growth of single graphene crystals and high resolution isotope labeling. Carbon **2017**, 111, 173–181.

37. Li, X.; Cai, W.; An, J.; Kim, S.; Nah, J.; Yang, D.; Piner, R.; Velamakanni, A.; Jung, I.; Tutuc, E.; Banerjee, S. K.; Colombo, L.; Ruoff, R. S. Large-Area Synthesis of High-Quality and Uniform Graphene Films on Copper Foils. Science **2009**, 324, 1312–1314.